

# CCD PHOTOMETRY OF GALACTIC GLOBULAR CLUSTERS. IV. THE NGC 1851 RR LYRAES

Alistair R. Walker

Cerro Tololo Inter-American Observatory, National Optical Astronomy Observatories<sup>1</sup>

## ABSTRACT

The variable star population of the galactic globular cluster NGC 1851(C0512-400) has been studied by CCD photometry, from observations made in the B, V and I bands during 1993-1994. Light curves are presented for 29 variables, seven of which are new discoveries. The behavior of the RR Lyraes in the period-temperature diagram appears normal when compared to clusters which bracket the NGC 1851 metallicity. Reddening and metallicity are re-evaluated, with no compelling evidence being found to change from the values of  $E(B - V) = 0.02$  and  $[Fe/H] = -1.29$  (Zinn scale) adopted in recent studies of the cluster. Photometry is provided for stars in an annulus with radii 80 and 260 arcsec centered on NGC 1851. To at least  $V = 18.5$  there is excellent agreement with the extensive earlier photometry for the brighter NGC 1851 stars, with systematics less than 0.02 mag in all colors. Instability strip boundary positions for several clusters shows a trend for the red boundary to move to redder colors as the metallicity increases.

keywords: globular clusters: individual (NGC1851) - RR Lyrae variable

## 1. Introduction

The galactic globular cluster (GC) NGC 1851 (C0512-400) is rich, centrally-condensed and belongs to the small group of clusters which display bimodal horizontal-branch (HB) morphology, defined (Catelan et al 1998) as having fewer RR Lyrae stars than either blue or red HB stars. Canonical theory, that is considering a GC as a population characterized by a single age, constant abundance and a red-giant branch (RGB) mass loss parameter that has a narrow Gaussian distribution (typically  $\sigma_M \sim 0.02M_\odot$ ), cannot explain such unusual HB morphology.

---

<sup>1</sup> Operated by the Association of Universities for Research in Astronomy, Inc., under cooperative agreement with the National Science Foundation.

In order to account for the bimodality, attention has focussed recently on scenarios which can alter the mass loss parameter, such as tidal stripping of red-giant envelopes in dense environments, rapid rotation, stellar encounters, and binary interactions. Sosin et al (1997) discuss these various options in the context of the most extreme example known of a GC with bimodal HB, NGC 2808, which displays a blue HB with multiple gaps that extends to below the main sequence turnoff in the  $V, B - V$  color-magnitude diagram (CMD),  $M_V \sim 5$ . They conclude that none of the present explanations are a satisfactory match to the observations. However, Sweigart & Catelan (1997) have modeled the unusual HB morphology of the metal rich GC's NGC 6338 ( $[Fe/H] = -0.60$ ) and NGC 6441 ( $[Fe/H] = -0.53$ ) for which Rich et al (1997) have obtained CMD's using the Hubble Space Telescope. Both clusters have HB's which slope upwards (brighter) with decreasing  $B - V$ , and have extended blue tails. Models with high helium abundance, rapid rotation, and helium mixing into the envelope are all able to produce a sloping HB morphology, and sometimes a bimodal distribution. The helium mixing alternative is particularly interesting given the observed heavy-element abundance variations in globular cluster red-giant stars (Kraft 1994). Mixing deep enough to produce enhanced aluminium, as observed in some stars, will also dredge up helium. Extensive deep mixing might be expected to destroy the sharp boundary corresponding to the deepest penetration of the convective zone, and thus prevent the observational pile-up of stars on the RGB near the level of the HB. NGC 1851 in fact appears to have quite a prominent such clump, thus suggesting that deep mixing has not taken place on the RGB at a luminosity less than that of the clump. Notwithstanding, the number of possible options still available to explain the peculiar NGC 1851 HB is considerable.

The CMD of NGC 1851 has most recently been studied by Walker (1992) (hereafter W92) in the  $B$  and  $V$  bands, in the UV by Parise et al (1994) and in the  $V$  and  $I$  bands by Saviane et al. (1997) (hereafter S97), where references to earlier work can be found. In both optical studies the bimodal HB is interpreted as a consequence of differing efficiencies of mass loss as the stars evolve up the RGB. W92 suggested that a unimodal mass distribution might be able to produce a bimodal HB stellar distribution when the detailed shape of the evolutionary tracks was taken into account, however S97 do not find good agreement when comparing with the Bertelli et al. (1994) tracks. They prefer a bimodal mass loss distribution, and indeed find some evidence to suggest that the radial distributions of the blue and red HB stars differ, pointing towards some as yet unexplained interaction between the dynamical evolution and the stellar evolution of these stars. On the other hand, Catelan et al (1998), using updated (Sweigart 1997) Sweigart and Gross (1976, 1978) models, find they can reproduce the NGC 1851 HB morphology with a unimodal, albeit very wide, mass distribution having characteristics  $\langle M_{HB} \rangle = 0.665M_{\odot}$  and  $\sigma_M = 0.055M_{\odot}$ .

Stetson et al. (1996) and Sarajedini et al. (1997) review the question of the relative ages of globular clusters, to reach very different conclusions. In both cases the HB level of NGC 1851 (W92) is used to link the second-parameter pair NGC 288 and NGC 362. Critical to these arguments is the  $V$  magnitudes of the reddest BHB stars and the RR Lyraes; the latter will be provided here for the first time.

Lying in the region of the HB which is sparsely populated, the RR Lyraes may provide important clues to help explain the reason for the bimodal HB, given the constraints that the pulsation properties place on stellar evolutionary status. There have been suggestions (Catelan 1997) that the 1851 variables are peculiar with respect to their behavior in the period-temperature diagram and that the photographic studies, as detailed below, also show that several of the RRab stars have light curve amplitudes near 2 magnitudes, much larger than normal.

Sawyer Hogg (1973) lists 10 variables in NGC 1851, from discoveries by Bailey (1924) and Laborde and Fourcade (1966). Preliminary periods for some of these stars, and an additional four new discoveries, resulted from a short observing campaign by Liller (1975) using photographic photometry at the CTIO 1.0-m and 1.5-m telescopes. She noted that V2 and V8 appeared to be constant, and V9 was very red. Wehlau et al. (1978) (hereafter W78) measured an additional 57 plates, almost all taken with the 1.0-m Swope telescope at Las Campanas, and analysed them along with the Liller (1975) plates. Periods were derived and light curves presented for a total of 19 RR Lyrae stars, the mean period of the RRab stars being 0.573 days, and the ratio of the number of RRc to RRab variables was found to be 0.36, both are values typical of an Oosterhoff type I system. The photometric zeropoint calibration for these observations was very uncertain, due to the lack of a definitive photometric sequence in the field. Stetson (1981) found four additional variables and two apparently constant stars lying in the instability strip. Wehlau et al. (1982) (hereafter W82) studied these stars using their original plate material supplemented with another 18 plates taken in 1970, whereupon three stars were found to be RR Lyraes, a fourth was classified as a probable field W UMa star, while a fifth is a red variable. W78 and W82 determined accurate periods and approximate mean  $\langle B \rangle$  magnitudes for all the stars they identified as RR Lyraes, classifying 15 stars as RRab and seven as RRc. The light curves display the 0.1 – 0.2 mag scatter typical for the photographic technique.

No modern studies of the NGC 1851 variables appear in the literature, however S97 identify an additional seven candidate RR Lyrae variables from a comparison of their photometry with that of W92, selecting stars with deviant photometry and  $V \sim 16, V - I \sim 0.4$ . Here we present new CCD photometry for the NGC 1851 RR Lyrae variables and compare with results for RR Lyraes in other GC's in this program (IC 4499,

M68, M72, NGC 6362).

## 2. Observations and Data Reduction

All observations were made using the CTIO 0.9-m telescope and Tektronix 2048 #3 CCD, during five observing runs in 1993 and 1994. NGC 1851 was approximately centered on the CCD and exposures taken in order  $V, B, I$ . Exposure times were always 300s, 600s, and 300s respectively, with the CCD being read out through either two or all four amplifiers simultaneously, using an Arcon CCD controller. Field size was 13.6 x 13.6 arcmin with pixel scale 0.40 arcsec. Further observational parameters are listed in Table 1, a total of 126 frames in each color were reduced. It should be noted that although the same filter set was not used throughout, the components for the  $B$  and  $V$  filters came from the same melts and the resulting filters have near identical passbands. Similarly, the two  $I$  filters are also near identical. On each photometric night several standard fields were observed (Landolt 1992).

The raw CCD frames were processed by zero-level (bias) subtraction followed by flat field division, the flats being short exposures of the twilight or dawn sky. Calibration frames were built from combinations of several individual frames with clipping of cosmic rays and interpolation over bad columns. All exposure times were sufficiently long that the center to corner shutter timing error was  $\ll 1\%$ . These procedures produced object frames with the sky flat to better than 0.5% in all filters.

Stars were identified and measured using DAOPHOT and ALLSTAR (Stetson 1987, 1995). Due to the large number of frames, the reduction programs were run in batch mode, via a script. The input to this script consisted a list of frames, the full-width at half-maximum (fwhm) of a typical star profile for each frame, the approximate x and y coordinates of the cluster center, and radii of an annulus which excluded the crowded stars near the cluster center. For NGC 1851 potential point-spread function (psf) stars closer than 90 arcsec from the cluster center were rejected. Each frame was then processed in turn by the script. The input fwhm was directly utilized in the “find” algorithm, and also used to generate the fitting radius and size of the sky annuli for ALLSTAR, and the size of the box for the psf stars. The “pick psf” routine was modified to only accept 200 – 300 candidate psf stars from the specified annulus. The initial pass through the frame produced a list of stars and determined an approximate psf, chosen to be a Moffat function plus look-up table of residuals, permitted to vary linearly with position on the frame. ALLSTAR was then run, followed by subtracting all the fitted stars with the exception of the psf stars. A new psf was determined, this time allowed to vary cubically with position, and extra stars not found on the first pass through the data were added to the star list. ALLSTAR was then

re-run on this larger list, utilizing the iterated psf. In conditions of good transparency, these procedures typically measured between 4000 and 15000 stars on each frame, depending on the seeing which critically affected the number of stars measured near the cluster center. Away from the central regions the magnitude limit was typically  $V \sim 21$ , approximately five magnitudes below the level of the HB. Examination of the star-subtracted frames output from the final pass through ALLSTAR showed good removal of the fitted stars, even those afflicted with severe coma near the corners of the CCD frames. This was particularly true for the June 1995 observations, which followed repairs to the 0.9-m telescope primary mirror radial supports and consequent improvement in image quality.

Matching up of all the approximately 3 million measurements was achieved using the programs DAOMATCH and DAOMASTER (Stetson 1995), which produced lists of stars for each frame, with their photometry, on a common numbering system. At this stage color equations (Table 2) and zeropoint adjustments were applied for each trio of  $V, B, I$  frames, via a set of local standards. On each photometric night sufficient Landolt (1992) fields were observed to measure color equation coefficients, extinction coefficients and zeropoints. The formal errors on the latter are typically a few millimags in each of  $V, B - V$  and  $V - I$ , and calibration errors arising from the standard star photometry alone should not exceed 0.01 mag for stars of normal colors ( $B - V \sim 0 - 1.5$ ). The success in transferring aperture photometry of the local standards on the NGC 1851 frames, measured in exactly the same way as the primary standards, can be ascertained best by comparisons of results from frames taken on different nights and different runs, often under conditions of very different seeing. The local standards have already been chosen to be relatively bright and as uncrowded as possible, so there should not be systematic differences between aperture and psf photometry due to faint stars in the star aperture. In both aperture and psf photometry faint stars in the sky background have little effect for these bright stars, avoiding most of the problems involved with sky determination (eg Stetson 1987). Notwithstanding, linking the local standard magnitudes to the primary standards is generally acknowledged to be the step most likely to introduce systematic calibration errors, and is perhaps best checked by comparing with completely independent sets of photometry.

There is extensive accurate photometry for stars in the region of NGC 1851. For  $V$  and  $B - V$ , W92 found from inter-comparisons between his own photometry of five bright stars near NGC 1851 with that by Stetson (1981), Alcaino et al. (1987), Sagar et al (1988), and Da Costa and Armandroff (1990) ( $V$  only) that agreement for  $V$  and  $B - V$  is no worse than 0.01 – 0.02 mag for all these measurements, and in particular the zeropoint offset between the W92 and the Stetson (1981) photometry is  $0.00 \pm 0.01$  mag for both  $V$  and  $B - V$ . On the basis of this excellent agreement he chose a set of 15 – 18 mag stars as local standards. Here, due to the smaller telescope aperture, we prefer to use brighter local

standards ( $V = 13 - 15$ ) although there are some stars in common. Apart from the present photometry, we have  $V, V - I$  photometry by S97, Da Costa and Armandroff (1990) and Alcaino et al (1987, 1990, hereafter A90).

We see no reason to alter the  $V$  and  $B - V$  zeropoints as used by W92, as the new calibrations reproduce the W92  $V$  and  $B - V$  zeropoints to within  $\pm 0.01$  mag. The situation with respect to the  $V - I$  photometry is more complicated. The  $V - I$  calibrations from the present data set reproduce both the bright A90 stars and the fiducial RGB of Da Costa and Armandroff (1990) to within  $\pm 0.01$  mag. The A90 fiducial for the lower RGB, subgiant branch and MS lies a mean of 0.02 mag redder than the present sequence to as faint as  $V = 20.5$ . S97 state that their  $V$  magnitude zeropoint agrees with W92, nominally to  $0.001 \pm 0.001$  mag (internal error), and with similar good agreement (0.012 mag) with A90. However when they compare their  $V - I$  zeropoint with A90 they find an offset of  $0.035 \pm 0.004$  mag in the sense that S97 are redder. Now S97 state that their external calibration errors are 0.03 mag in  $V$  and 0.02 mag in  $I$ , so the  $V$  agreement may be fortuitous and the  $V - I$  zeropoint offset is only slightly larger than a one sigma error. The present  $V - I$  measurements when compared to S97 actually show good agreement (to 0.01 mag or better) for the HB and on the RGB to the level of the HB. Fainter than this there are systematic offsets between S97 and both A90 and the present work, which grow larger at fainter magnitudes in the sense that S97 is redder. On the MS at  $V = 20$ , S97 is 0.07 mag redder than A90 and 0.08 mag redder than here. Now S97 has significantly better image quality (seeing 1.1 - 1.2 arcsec) for their frames, albeit with rather short exposure times, and so the source of the non-linearity is not certain. An indication might be that somewhat similar behavior is seen when comparing the B-V colors of the MS here with those of W92, where W92 is redder by 0.02-0.03 mag despite excellent agreement for brighter stars. In any case, the systematic trends at faint magnitudes are irrelevant for the present work, and in fact it is gratifying that the agreement for HB and brighter stars is so good. NGC 1851 is a cluster with high central concentration, and ground-based photometry within an arc minute of its center is difficult, even with excellent seeing.

To summarize, we believe that the  $V$ ,  $B - V$ , and  $V - I$  magnitude zeropoints are known to better than  $\pm 0.02$  mag, and probably to  $\pm 0.01$  mag. The various sources of CCD photometry agree well with each other to  $V \sim 18.5$ , but fainter than that some systematic trends with magnitude occur.

### 3. RR Lyrae Photometry

Candidate variable stars were identified using the Welch & Stetson (1993) method, which looks for correlated changes in near-simultaneous measurements made at two wavelengths. Since we have observations made near-simultaneously at three wavelengths, the *variability index* was rewritten as

$$I \propto \sum_i \delta B \delta V \delta I$$

where the  $\delta$  magnitudes are the differences with respect to the mean. In order to strengthen discrimination against “bad” measurements biasing the variability index, recognition was taken of the fact that for RR Lyraes the amplitude ratios in the three filters are on average  $B : V : R = 1.0 : 0.8 : 0.5$  thus the delta magnitudes were required to obey this condition, with generous limits, otherwise the observation was rejected. Thus not only must variations at a given time be correlated between the three colors, but the ratios of the variations in each band must be reasonable.

At the same time, mean magnitudes were calculated for all the stars. Weighting the individual results via the photometric errors returned by ALLSTAR is not a useful technique for calculating mean magnitudes in such a crowded field, where the major source of scatter is incorrect measurements of blended stars, particularly on the poorer-seeing frames. Instead, residuals about an initial mean were calculated, and the most deviant values discarded. This process was iterated, until convergence was achieved with more than half the measures remaining, otherwise the star was discarded. Table 3 includes all stars measured brighter than magnitude  $V = 19$  and contained within an annulus of radii 80 and 260 arcsec centered on the cluster.

The program produced a list of variable stars, prioritized by the *variability index*. The stars were then subject to period-finding using a phase-dispersion minimization program and a least-squares fitting periodogram program, both written originally by Dr L A Balona (SAAO). As a result of these procedures all 22 previously known RR Lyrae variables were re-discovered, along with another seven additional stars, six RRab and one RRC. The mean period of the RRab stars increases slightly, to 0.586 days, and the ratio RRC:RRab is now 0.38. The new discoveries are numbered V27 through V33. We confirm (W78, W82) that V2, V9 and V24 are red stars, and that V25 is a likely field W UMa variable. The full CCD field (13.6 arcmin square) is shown in Figure 1, with the more distant RR Lyraes identified. Figure 2 shows a 100 arcsec square field centered on the cluster, with the inner RR Lyraes marked. Photometry within 30 arcsec of the cluster center has large systematic errors and a CMD for these stars shows much scatter. Notable is star no. 17, only 25

arcsec from the cluster center, and which can be identified on Figure 2 as the bright star 7 arcsec N and 1.6 arcsec W of V31. This star has  $V = 13.21$ ,  $B - V = -0.07$ ,  $V - I = -0.12$  and is UV-5 (Vidal & Freeman 1975) a radial velocity member and thus a star in the post-asymptotic giant branch (PAGB) stage of evolution, (see S97 figure 6). S97 identified several “supra-HB” candidates but most of these are well-distant from the cluster, and will require membership confirmation. No bright stars with  $B - V < 0.6$  are here found within 4 arcmin of the cluster center, and indeed two other PAGB candidates (UV-6, UV-7) have already been shown to be radial velocity non-members (Da Costa 1982).

The high concentration of NGC 1851, coupled with the fact that only 206 stars, mostly brighter than the HB, were able to be measured within 25 arcsec of the cluster center, means that it is certain that more RR Lyraes exist in the very crowded central regions. Their discovery will require much better image quality than the 1.3 – 1.8 arcsec fwhm typical for the stars on the frames available here. Of the seven stars suggested by S97 as candidate variables, three are amongst the seven new variables mentioned above, while the other four stars are constant. Two of the latter are close ( $\sim 1$  arcsec) doubles.

The RR Lyrae  $V$  magnitude light curves are plotted as a function of phase in Figure 3. In almost all cases period-finding was straight-forward, however several stars show poor-quality light curves, particularly those nearer to the cluster center. In particular, V30 shows point-point scatter of more than 0.1 mag and the two longest period RRc stars, V19 and V33, are scarcely better. The shortest period RRc star, V23, appears to have variable amplitude, while the RRab stars V5, V29 and V28 probably display the Blazkho effect. V10 proved to be particularly troublesome. It has a period by W78 of 0.49948 days but this does not fit the present data set, and 0.49975 days is preferred. This fits the data better, but not perfectly, and several other candidate periods were investigated, with no success. Aliasing is a problem, and a period near 0.333 days is also possible. The rather low amplitude of the light curve would support this choice, but the color of the star and the better fit of the chosen period would appear to rule out this possibility. A long period RRab option, which would be consistent with both colors and amplitude, does not seem possible from examination of the power spectrum. Three stars have photometry severely contaminated by close companions, these are V14 which is brighter than expected, and has a clearly elliptical profile, while star V30 is very crowded, being only 15 arcsec from the cluster center. Star V19 is also rather bright, with a fainter close companion, and photometry for all these stars should be treated with caution. Individual measurements for the RR Lyraes are given in Table 4, which lists the heliocentric Julian date corresponding to the midpoint of the  $V$  exposure, the corresponding phase with arbitrary zero, the additive offsets in days to the midpoints of the B and I exposures, the  $V, B, I$  magnitudes, and the errors in the  $V, B$  and  $I$  magnitudes.



The data set are not optimal for finding other than short period variables, although stars varying on timescales of months can be noticed when observations from the different observing runs are compared. Five such stars at the tip of the RGB were found to be variable, with pseudo-periods of timescale a year and amplitudes of 0.1 – 0.2 mag. No variable blue stragglers were found.

#### 4. RR Lyrae Derived Quantities

The technique of deriving astrophysical quantities from Fourier decomposition of the light curves of RR Lyrae stars was pioneered by Simon (1988). Simon and Clement (1993) compared their hydrodynamic models with Fourier parameters for RRc stars and derived expressions evaluating mass, luminosity, temperature and relative helium abundance. Jurcsik and Kovács (1996) and Kovács and Jurcsik (1996) found relationships between the Fourier parameters of RRab stars and their metallicity and luminosity. These results have recently been tested against observations of RR Lyraes in seven galactic GC's by Clement and Shelton (1997). The derivation of luminosities from the Fourier coefficients for the NGC 1851 and other GC RR Lyraes will be discussed in detail elsewhere (Kovács and Walker, work in progress). Fourier series were fitted to the light curves, to evaluate intensity- and magnitude-mean magnitudes, mean colors, amplitudes, as well as the Fourier amplitude and phase coefficients, as described by Walker (1994). We have calculated coefficients for all three ( $V, B, I$ ) lightcurves, which allow assessment of the coefficient errors independent of the formal errors returned by the fitting program, which are also tabulated. Intensity mean magnitudes, mean colors, and amplitudes are listed in Table 5, while Table 6 contains the magnitude means, the Fourier phase coefficients and combinations. The very large amplitudes found for some stars (eg V1, V8, V16) by W78 are not confirmed. We note that their photographic photometry is based on a photoelectric sequence by Alcaïno (1971) that has some uncertainties at the faint end, which is itself a magnitude brighter than the RR Lyraes at minimum light. For stars brighter than  $B \sim 16$ , the photographic photometry shows good agreement with the CCD work, but is fainter by 0.5 mag by  $B \sim 17$ . This is mostly likely due to an incorrect calibration of the photographic plates when extrapolating from the fainter photoelectric sequence stars.

Bono et al. (1995) have calculated corrections to observed mean colors to obtain the color of the equivalent static atmosphere, as a function of light-curve amplitude. For the static mean  $V$  magnitude, the corrections to be applied to the intensity mean magnitudes  $\langle V \rangle$  in Table 5 are very small, even for the highest amplitude RRab star, V1, the correction is only -0.01 mag. It is worthwhile to note that the correction required to the

magnitude mean  $V$  for this star is  $-0.08$  mag. If these corrections are applied, then in both cases the equivalent static  $V$  magnitude is  $16.04$ , a gratifying result. The corrections required for  $(B - V)_{mag}$  are also not large. RRab stars with amplitudes  $A_B$  in the range  $0.7 - 1.4$  mag need a correction of  $-0.01$  mag, rising to  $-0.02$  mag by  $A_B = 1.7$  mag. For the very low amplitude RRc star the correction is  $+0.008$  mag, for all other RRc stars the correction is within a few millimags of  $-0.005$  mag.

The question of how to convert between RR Lyrae colors and effective temperatures  $T_e$  is a vexing one. The first step, that of calculating the correct mean color from those observed, has been dealt with in the preceding paragraph. Kurucz (1992) calculated colors as a function of  $[Fe/H]$ ,  $T_e$ , and  $\log g$  from model atmospheres, and these tables have been widely used. For RR Lyraes, Sandage (1981) first suggested that the blue amplitude  $A_B$  measured relative temperatures for RRab stars, and this approach was extended by Carney et al. (1992) who found a relationship  $T_e = f(A_B, [Fe/H], P)$  best represented temperatures for their sample of RRab stars. Catelan et al. (1998) argue that a relationship independent of  $P$  is preferable, and show that their temperature scale is in excellent agreement with the Carney et al. (1992) temperatures. However the use of this relation in period-shift analyses shows much more scatter than if Carney et al. (1992) temperatures are used. Castellani and de Santis (1994) note that the metallicity dependence is slight, and prefer to define their temperature scale in terms of  $P$  and  $A_B$  alone. In general, these relations are not very robust given the number of parameters compared to the calibrating stars. It thus seems preferable to use the colors directly, and recently Castelli, Kurucz, and Gratton (1997a,b) (hereafter C97) have provided calibrations based on revised model atmospheres. McNamara (1997) has carefully compared consistency between the temperatures so predicted from various colors, and the consequently derived gravities and luminosities. He concludes that the optical colors best correspond to “correct” effective temperatures, and that the oft-used V-K scale is systematically offset. The optical temperature scale is some 200-300 K hotter for a given color than the older Kurucz (1992) scale, and he goes on to show that the higher temperatures and consequent higher luminosities are consistent with a distance modulus of  $18.53$  mag for the Large Magellanic Cloud, similar to that given by other distance indicators. We will use the C97 temperature scale here, interpolating in the provided table to  $[Fe/H] = -1.29$  and  $\log g = 2.75$  (Fernley 1993), relevant for the NGC 1851 RR Lyraes. The B-V colors will be used to best allow comparisons with earlier work.

## 5. Reddening and Metallicity

It is convenient to deal with reddening and metallicity together, since most photometric methods do not determine these two quantities independently. W92, after an extensive discussion of the available reddening measurements, concluded that there was very little evidence to support the sometimes rather high values suggested by some workers, and adopted  $E(B - V) = 0.02 \pm 0.02$ . In similar manner, W92 found  $[Fe/H] = -1.29 \pm 0.07$ , as advocated by Da Costa and Armandroff (1990), was consistent with the new photometry. S97 adopted the same value, which is on the Zinn and West (1984) scale, used here for consistency with previous work. Rutledge et al. (1997), in their discussion of GC  $[Fe/H]$  derived from measurements of the Ca II triplet lines, find that the recent Carretta and Gratton (1997) metallicity scale gives  $[Fe/H]$  values some 0.2 dex more metal rich than the Zinn and West (1984) scale for clusters with metallicity similar to NGC 1851. They also conclude that it is not at all obvious which of the two scales best measures  $[Fe/H]$ .

As noted earlier by Armandroff and Da Costa (1990), the Ca triplet measurement for NGC 1851 lies 0.15 dex off the calibration defined by other GC if  $[Fe/H] = -1.29$  is assumed, by approximately 0.15 dex, in the sense that the Ca triplet measurements suggest a more metal rich value. Whether this represents enhancement of  $[\alpha/Fe]$  relative to the other GC that calibrate the Ca triplet metallicity scale, or incorrect observations, would be important to resolve with a new spectroscopic determination.

We can measure the reddening and metallicity here from the position of the RGB in the  $V, V - I$  CMD (Sarajedini 1994), or in the  $V, B - V$  CMD (Sarajedini and Layden 1997), and also calculate the reddening via Sturch’s method (Sturch 1966, Walker 1990, Blanco 1992) applied to the RRab variables.

We use Sturch’s method as described by Walker (1990), where the reddening zeropoint has been adjusted to correspond to zero reddening at the galactic poles and the  $[Fe/H]$  scale is that of Zinn and West (1984), whereby

$$E(B - V) = (B - V)_{min} - 0.24P - 0.056[Fe/H] - 0.336,$$

where  $(B - V)_{min}$  refers to phases 0.5 – 0.8 and is applicable for RRab stars only. For 13 stars with  $\sigma(B - V)_{min} < 0.04$  mag, and with  $[Fe/H] = -1.29$ ,

$$E(B - V) = 0.05 \pm 0.02.$$

This is 0.03 mag higher than that determined by W92. It should be noted however that in two other clusters studied in this series, M68 (Walker 1994) and IC 4499 (Walker and Nemeč 1996),  $E(B - V)$  found by Sturch’s method was in both cases 0.02 mag larger than the final adopted mean from several methods. An alternative calibration by Blanco

(1992) also produces reddenings smaller by about 0.015 mag. The present result, although suggesting a slightly higher reddening for NGC 1851 than found by Walker (1992), should not be afforded excessively high weight due to these zeropoint uncertainties.

Sarajedini (1994) introduced a method to determine  $E(V - I)$  and  $[Fe/H]$  simultaneously, from the position and shape of the RGB in the  $V, V - I$  CMD. The method is calibrated from six GC, one of which happens to be NGC 1851, from photometry by Da Costa and Armandroff (1990). Given that our photometry of the NGC 1851 RGB reproduces that found by Da Costa and Armandroff (1990), applying their method just forces NGC 1851 to fall exactly on the Sarajedini (1994) calibration fiducials, with  $[Fe/H] = -1.4 \pm 0.2$  and  $E(B - V) = 0.02 \pm 0.02$ , where  $E(V - I) = 1.25E(B - V)$ . Similarly, Sarajedini and Layden (1997) use NGC 1851 data from W92 as one of their primary calibrators in the  $V, B - V$  version of the method. In this case the position of NGC 1851 relative to the fiducials would argue for little change in the nominal  $[Fe/H]$  and  $E(B - V)$  values.

Finally, we can calculate  $[Fe/H]$  from the Fourier decomposition of the RRab light curves. The cluster metallicity can be derived from the Fourier coefficients of the RR Lyraes (Jurcsik and Kovács 1996). who derive a linear relation between  $[Fe/H]$ , Period  $P$  and the Fourier phase parameter (see Simon 1988)  $\phi_{31}$ ,

$$[Fe/H] = -5.038 - 5.394P + 1.345\phi_{31}.....(1)$$

where because of the  $2\pi$  ambiguity the phase should be taken closest to the sample average, 5.1. Note that Simon (1988) decomposes the Fourier series as cosines (as are the values in Table 6) whereas Jurcsik and Kovács (1996) prefer a sine decomposition. To convert from cosine to sine decomposition requires subtracting  $\pi/2$ ,  $3\pi/2$ , and  $5\pi/2$  respectively from the phase combinations  $\phi_{21}$ ,  $\phi_{31}$  and  $\phi_{41}$ . We proceed by choosing the nine RRab stars with the best light curves, and weight  $\phi_{31}$  found from each of  $B$  and  $V$  twice that of the  $I$  result, since the lower amplitude  $I$  light curves always give a much larger error for  $\phi_{31}$  than do  $B$  and  $V$ . It is found that

$$[Fe/H] = -1.31 \pm 0.05 \text{ (s.e.)}.$$

In this case the  $[Fe/H]$  scale is that described by Jurcsik (1995), which is based on high dispersion spectroscopy rather than the Zinn and West (1984) scale. An approximate conversion to the Zinn and West (1984) scale follows from noting that M4 has  $[Fe/H] = -1.28$  on the latter scale, while four independent high dispersion spectroscopy measurements give mean  $[Fe/H] = -1.11$ . This suggests that the metallicity on the Zinn and West (1984) scale for NGC 1851 is near  $[Fe/H] = -1.45$  via equation (1).

In summary, the new estimates for the metallicity and reddening of NGC 1851 are close to the values of  $[Fe/H] = -1.29 \pm 0.07$  and  $E(B - V) = 0.02$  adopted by W92 and S97, and these values will be retained for this paper. The question of the *true* GC  $[Fe/H]$  scale is obviously a very important one, and given that the Zinn and West (1984) and Carretta and Gratton (1997) scales differ non-linearly, ramifications when comparing stellar properties between clusters of differing metallicities will be pervasive (Jucsik 1995).

## 6. Period Shift

We exclude V14 from this analysis as its magnitude is clearly discrepant, see above. Temperatures were calculated from C97 models, as described above, then periods for the first overtone pulsators were adjusted to the equivalent fundamental period by the addition of 0.125 to  $\log P$  (van Albada & Baker 1971). A further correction, to compensate for the period change due to evolution in luminosity, is usual. Brocato et al. (1996) argue that the ZAHB should be the reference luminosity for this correction, rather than the mean magnitude (Sandage 1990). The latter has the disadvantage of being sample dependent, although simple to calculate, whereas care is needed to observationally define the ZAHB position correctly. With a reasonable sample of RR Lyraes, as is the case here, the ZAHB can be accurately defined. A mean of the faintest 11 stars is  $V = 16.115 \pm 0.002$  (internal error), and a true lower bound would be only 0.01 mag fainter. For comparison, we will use the photometry and periods determined for M68 (Walker 1994), IC 4499 (Walker & Nemeč 1996) and NGC 6362 (in preparation), calculating periods and temperatures in the same way as described for NGC 1851. For M68,  $V_{ZAHB} = 15.702 \pm 0.005$ , for IC 4499  $V_{ZAHB} = 18.29 \pm 0.01$ , and for NGC 6362  $V_{ZAHB} = 15.33 \pm 0.01$ . Period-shift diagrams are plotted in Figure 4. The observational uncertainty mostly affects the temperature axis, as in all these clusters the ZAHB can be well-defined, and an (unlikely) error of placement of the ZAHB of 0.03 mag corresponds to only a displacement of 0.01 in  $\log P$ . Once the ZAHB is chosen, magnitude measurements are differential. The major source of observational error occurs in the calculation of the temperature, where an error of 0.01 in  $\log T$  corresponds to 0.03 mag in the B-V color, which must first be corrected for reddening. The figure shows no period shift between IC 4499 and NGC 1851, and only an insignificant indication of a shift between these two clusters and NGC 6362. Since NGC 6362 and IC 4499 bracket NGC 1851 in metallicity, we conclude from this diagram that the period-shift behaviour of the NGC 1851 variables appears normal. On the contrary, the M68 variables have a substantial period-shift when temperatures are calculated using  $E(B-V) = 0.07$ , as was found by Walker (1994) when comparing to the OoI cluster M3 using a different color-temperature calibration (Sandage 1990). The shift could be completely removed if the M68 reddening

was reduced to  $E(B - V) = 0.03$ , the value favoured in the Brocato et al. (1994) study of M68 (see Figure 4). Walker (1994) provided several reasons why the higher value is to be preferred, but re-evaluations by Gratton et al. (1997) and especially by Brocato et al. (1997) would argue for a value of  $E(B - V) = 0.04 \pm 0.01$ . Gratton et al. (1997) also prefer a slightly higher metallicity for M68,  $[Fe/H] = -2.0$ , but the 0.1 dex change has an insignificant effect on the temperatures. Final resolution of the M68 reddening question would appear to require further observational effort.

## 7. CMD morphology

The CMD in general has been described by W92 and S97, the latter also include a pre-COSTAR HST CMD of the cluster center. A more recent HST CMD of the central region of NGC 1851 is presented without discussion by Sosin et al (1997). These CMD's are all deep enough to show stars well below the MS turn-off. In Figure 5 we plot all stars measured brighter than  $V \sim 20.5$  in an annulus with radii 80 and 260 arcsec, while Figure 6 adds all measured stars to within 30 arcsec of the cluster center. This includes all the known RR Lyraes except V30 which is only 15 arcsec from the cluster center. Both diagrams show only a few field stars well-distanced from the cluster principal sequences, so field star contamination is not an issue when interpreting these diagrams. As expected, Figure 5 shows fewer blends scattered off the principal sequences.

The RGB is well-populated and clearly separated from the asymptotic giant branch (AGB). At fainter magnitudes, and at bluer colors than the MS, are a number of blue stragglers, which are extensively discussed by S97. The MS itself is well-defined, by considering the Figure 5 stars with  $19.6 < V < 19.1$ , then  $\sigma(B - V) = 0.015$  mag for a best-fit Gaussian, only slightly larger than the mean internal photometric error for these stars of 0.009 mag. The true external scatter due to photometric errors will be larger than this figure by some not well-determined amount, even though the increase in color dispersion arising from blends and binaries is minimized by choosing the near-vertical part of the MS where blending MS stars all have very similar colors and thus contribute little to the color dispersion. Adding 0.005 mag in quadrature to the internal errors restricts the possible intrinsic width of the MS to the equivalent of a range in metallicity of approximately 0.1 dex. A larger and probably more realistic internal to external error correction effectively allows for no dispersion in metallicity, which is also the conclusion reached by S97.

The HB shows a very condensed clump of red HB stars, with a pronounced gap on the red side. Several stars are loosely grouped above and slightly to the red of the red HB, these stars are presumably in a state of evolution at the very end of, or beyond,

core helium burning. One or two of these stars may be evolved blue stragglers. The star density falls steadily bluewards along the HB, reaching a minimum in the vicinity of the RRc stars, before increasing again with an extensive tail of blue HB stars extending to  $V \sim 17, B - V = -0.05$ . A well-measured, very blue star at  $V = 18.46, B - V = -0.132$  is only 120 arcsec from the cluster center and thus has a good probability of being a member. This star (UIT 31) is one of two with very blue UV colors (Parise et al 1994), indicative of temperatures well in excess of 10000 K. The second star (UIT 44) has even bluer UV color than UIT 31, but Landsman (1994) found rather unremarkable optical colors ( $V = 18.6, B - V = 0.11$ ) and confirmed the star as being a radial velocity member of NGC 1851. He suggested that perhaps the star was a binary, and indeed a combination of a star near the MS turn-off ( $V = 19.2, B - V = 0.6$ ) when subtracted from the optical colors gives  $V = 19.5, B - V = -0.3$ , much more consistent with the UV colors and the optical spectra, both of which indicate a temperature near 30000 K.

The ZAHB is very cleanly defined, and is not *horizontal*, being slightly brighter at bluer colors. This is best seen in Figures 7 and 8, where the ZAHB appears to slope steadily upwards towards the blue, from  $V = 16.20$  at  $B - V = 0.65$  to  $V = 16.12$  at  $B - V = 0.20$ . Bluer HB stars become rapidly fainter for a small change in color, as  $B - V$  becomes insensitive to temperature changes and the bulk of the emitted radiation from these hot stars occurs in the UV. In Figure 7, four stars lie slightly above the blue HB, near  $V = 16.0, B - V = 0.08$ . Three of these stars are crowded. The fourth, which lies 111 arcsec from the cluster center and ought to be relatively uncrowded, actually has a red star almost two magnitudes brighter in  $V$  at 3 arcsec south, and a slightly fainter star at separation 1.5 arcsec west, so the photometry may well be incorrect. Apart from these stars, and the few RR Lyraes with unreliable photometry as discussed above, the vertical extent of the HB appears to narrow with bluer  $B - V$  colors. Catalan et al (1998) state that observations such as these constrain the theoretical paths of HB evolutionary tracks; they note that the Lee and Demarque (1990) tracks have longer blue loops for a given metallicity than do either their own tracks or indeed the later Yale tracks (Yi, Lee and Demarque 1995). Both of the latter agree much better with the observed HB star distribution in NGC 1851.

No significant gaps are apparent in the star distribution along the HB. The numbers of blue HB stars (B), compared to variables (V) and red HB stars (R) are:  $B : V : R = 31 : 15 : 64$  in a 30-80 arcsec annulus and  $B : V : R = 39 : 13 : 61$  in an 80-260 arcsec annulus. Assigning errors of  $\pm 2$  counts for the non-variables, and  $\pm 1$  counts for the variables, then we can compare relative numbers. For the whole sample, the Lee parameter  $(B - R)/(B + V + R) = -0.25 \pm 0.03$ . The ratio B:R in the inner zone is  $31 : 64 = 0.48 \pm 0.05$ , and in the outer zone  $39 : 61 = 0.64 \pm 0.05$ . The difference is barely significant. A more stringent investigation by S97 found that 2-population Kolmogorov-Smirnov tests indicated

that within 100 arcsec from the cluster center the RHB, BHB and SGB populations all had the same distribution but outside 100 arcsec the BHB stars appeared slightly less concentrated. We have also counted RGB stars, down to  $V = 16.0$  to avoid the clump stars. Generally, the AGB stars are easy to identify, and field contamination is negligible (Ratnutunga and Bahcall (1985)). We count 60 RGB stars in the 30-80 arcsec annulus, and also 60 stars in the 80-260 arcsec annulus, with an error of  $\pm 4$  stars each. We have included the very red star 59 ( $V = 13.39, B - V = 1.88, V - I = 1.89$ ) as a member, the next reddest star is 63 ( $V = 13.40, B - V = 1.58, V - I = 1.58$ ). The ratio of RGB stars in the two annuli is not significantly different from the corresponding ratios for the RHB and the BHB stars, although nominally closer to that for the RHB stars.

The edges of the instability strip, judged by the measured colors of variables near the strip boundaries, are  $(B - V)_0 = 0.19 \pm 0.01, (V - I)_0 = 0.235 \pm 0.01$  corresponding to the first overtone blue edge, and  $(B - V)_0 = 0.41 \pm 0.01, (V - I)_0 = 0.545 \pm 0.01$ , corresponding to the fundamental red edge. The RRc/RRab boundary is at  $(B - V)_0 = 0.29 \pm 0.02, (V - I)_0 = 0.365 \pm 0.02$ . These will first be compared with the results for some other clusters, and also with theory.

It has long been suspected (eg Deupree 1977) that the red edge of the instability strip moves to redder colors at higher metallicities. This has been difficult to confirm as the postulated shift is not large, comparable to the typical errors in reddening determinations. Instability strip boundary colors for several galactic and LMC clusters observed in similar manner to NGC 1851 are listed in Table 7. A least squares fit to the the colors of the red edge shows a shift of  $0.04 \pm 0.02$  mag/dex, over a metallicity range of approximately  $[Fe/H] = -1$  to  $-2$ . This is only a  $2\sigma$  result and data from more clusters are clearly needed. The corresponding temperatures can be derived from the C97 tables, assuming  $\log g = 2.75$  (Fernley 1993) and show that the temperature change is not large, falling from 6230 K to 6120 K. For reference, at fixed metallicity and gravity this temperature change would correspond to only 0.03 mag. By contrast, the color of the blue edge appears constant near  $B - V = 0.18$ , however the corresponding temperatures are 7300 K at  $[Fe/H] = -2$  and 7360 K at  $[Fe/H] = -1$ .

We can compare these results with theoretical predictions by Bono et al. (1997), who have calculated mode boundaries for  $Z = 0.02$  and  $Z = 0.0001$  models. The slope of their bolometric magnitude-metallicity relation is 0.24. Their metal-rich model has  $M = 0.53M_{\odot}$  and  $Y = 0.28$ , the metal-poor model has  $M = 0.65M_{\odot}$  and  $Y = 0.24$ . The lack of a model with  $Z = 0.001$  immediately makes what follows preliminary, given the large interpolation required. It is immediately obvious that there is a moderate difference in zeropoint between the predictions and transformed measurements, since for the red edge the Bono et al. (1997)



temperatures are some 300 K too low. The predicted temperature difference of 50 K is not too inconsistent with the 110 K measured, since at the red edge 0.01 mag corresponds to 35 K and there is at least an uncertainty at this level observationally.

At the blue edge of the instability strip, the Bono et al. (1997) predictions are approximately 100K too cool. Via the C97 transformations, a color of  $B - V = 0.18$  will correspond to a star with temperature 7360 K at  $[Fe/H] = -1$  and 7300 K at  $[Fe/H] = -2$ , the reverse sign to the Bono et al. (1997) prediction. Here 0.01 mag in  $B - V$  corresponds to 50 K, so again these results are not too discordant.

Finally, we investigate the color of the RRcd - RRab transition for clusters with sufficient stars of both groups that the position is well-defined. This color is listed in the final column of Table 7. The small trend visible, that the color of the transition reddens slightly at higher metallicities, runs counter to the trend that the temperature (C97) at constant color increases with metallicity, thus the transition occurs at near constant temperature, 6725 K, assuming  $\log g = 2.75$ .

Acknowledgements: I would like to thank Marcio Catelan for stressing the importance of the NGC 1851 RR Lyraes, and for pointing out the unusually large photographic amplitudes.

## REFERENCES

- Alcaino, G. 1971, *A&A*, 15, 360
- Alcaino, G., Liller, W., & Alvarado, G. 1987, *AJ*, 93, 1464
- Alcaino, G., Liller, W., Alvarado, F., Wenderoth, E. 1990, *AJ*, 99, 817 (A90)
- Bailey, S. 1924, *Harvard Bull.* no. 802
- Bertelli, G., Bressan, A., Chiosi, C., Fagotto, F., & Nasi, E. 1994, *A&AS*, 106, 275
- Blanco, V.M. 1992, *AJ*, 104, 734
- Bono, G., Caputo, F., & Stellingwerf, R.F. 1995, *ApJS*, 99, 263
- Bono, G., Caputo, F., Cassisi, S., Incerpi, R., & Marconi, M. 1997, *ApJ*, 483, 811
- Brocato, E., Castellani, V., & Ripepi, V. 1994, *AJ*, 107, 622
- Brocato, E., Castellani, V., & Ripepi, V. 1996, *A&A*, 111, 809
- Brocato, E., Castellani, V., & Piersimoni, A. 1997, *ApJ*, 491, 789
- Carney, B.W., Storm, J., & Jones, R.V. 1992, *ApJ*, 386, 663

- Carretta, E., & Gratton, R.G. 1997, *A&AS*, 121, 95
- Castellani, V., & de Santis, R. 1994, *ApJ*, 430, 624
- Castelli, F., Kurucz, R., & Gratton, R. 1997a, *A&A*, 318, 841 (C97)
- Castelli, F., Kurucz, R., & Gratton, R. 1997b, *A&A*, 324, 432 (C97)
- Catelan, M. 1997, private communication
- Catelan, M., Borissova, J., Sweigart, A.V., & Spassova, N. 1998, *ApJ*, in press, (astro-ph/9708174)
- Clement, C.M., & Shelton, I. 1997, *AJ*, 113, 1711
- Da Costa, G. 1982, *PASP*, 94, 769
- Da Costa, G.S., & Armandroff, T.E. 1990, *AJ*, 100, 162
- Deupree, R.G. 1977, *ApJ*, 214, 502
- Fernley, J.A. 1993, *A&A*, 268, 591
- Gratton, R.G., Fusi Pecci, F., Carretta, E., Clementini, G., Corsi, C.E., Lattanzi, M.G. 1997, *ApJ*, 491, 749
- Jurcsik, J. 1995, *Acta. Astr.*, 45, 653
- Jurcsik, J., & Kovács, G. 1996, *A&A*, 312, 111
- Kovács, G., & Jurcsik, J. 1996, *ApJ*, 466, L17
- Kraft, R.P. 1994, *PASP*, 106, 553
- Kurucz, R.L. 1992, in *IAU Symp. 149, The Stellar Populations of Galaxies*, ed. B. Barbuy & A. Renzini (Dordrecht:Kluwer), 225
- Laborde, J.R., & Fourcade, C.R., 1966, *Cordoba Repr.*, p. 138
- Landolt, A.U. 1992, *AJ*, 104, 340
- Landsman, W.B. 1994, in *Hot Stars in the Galactic halo*, ed. S.J. Adelman, A.R. Uggren, & C.J. Adelman (Cambridge: Cambridge University press), p. 156
- Lee, Y.-W., & Demarque, P. 1990, *ApJS*, 73, 709
- Liller, M.H. 1975, *ApJ*, 201, L125
- McNamara, D.H. 1997, *PASP*, 109, 857
- Parise, R.A., et al. 1994, *ApJ*, 423, 305
- Ratnutunga, K., & Bahcall, J.N. 1985, *ApJS*, 59, 63
- Rich, R.M., et al. 1997, *ApJ*, 484, 25

- Rutledge, G.A., Hesser, J.E., & Stetson, P.B. 1997, PASP, 109, 907
- Sagar, R., Cannon, R.D., & Hawkins, M.R.S. 1988, MNRAS, 232, 131
- Sandage, A. 1981, ApJ, 248, 161
- Sandage, A. 1990, ApJ, 350, 631
- Sarajedini, A. 1994, AJ, 107, 618
- Sarajedini, A., Chaboyer, B., & Demarque, P. 1997, PASP, 109, 1321
- Sarajedini, A., & Layden, A. 1997, AJ, 113, 264
- Saviane, I., Piotto, G., Fagotto, F., Zaggia, S., Capaccioli, M., & Aparicio, A. 1997, A&A, in press (S97)
- Sawyer-Hogg, H.B. 1973, Publ. David Dunlap Obs., 3, no. 6
- Simon, N.R. 1988, ApJ, 328, 747
- Simon, N.R., & Clement, C.M. 1993, ApJ, 410, 526
- Sosin, C., et al. 1997, ApJ, 480, 35
- Stetson, P.B. 1981, AJ, 86, 687
- Stetson, P.B., 1987, PASP, 99, 191
- Stetson, P.B., 1995, DAOPHOT II User's Manual
- Stetson, P.B., Vandenberg, D.A., & Bolte, M. 1996, PASP, 108, 560
- Sturch, C.R. 1966, ApJ, 143, 774
- Sweigart, A.V. 1997, ApJ, 474, L23
- Sweigart, A.V., & Catelan, M. 1997, preprint
- Sweigart, A.V., & Gross, P.G. 1976, ApJS, 32, 367
- Sweigart, A.V., & Gross, P.G. 1978, ApJS, 36, 405
- van Albada, T.S., & Baker, N. 1971, ApJ, 169, 311
- Vidal, N.V., & Freeman, K.C. 1975, ApJ, 200, 19
- Walker, A.R. 1990, AJ, 100, 1532
- Walker, A.R. 1992, PASP, 104, 1063 (W92)
- Walker, A.R. 1994, AJ, 108, 555
- Walker, A.R., & Nemec, J.M. 1996, AJ, 112, 2026
- Wehlau, A., Liller, M.H., & Coutts Clement, C. 1978, AJ, 83, 598 (W78)

Wehlau, A., Liller, M.H., Coutts Clement, C., & Wizinowich, P. 1982, AJ, 87, 1295 (W82)

Welch, D., & Stetson, P.B. 1993, AJ, 105, 1813

Yi, S., Lee, Y.-W., & Demarque, P. 1995, ApJ, 411, L25

Zinn, R., & West, M.J. 1984, ApJS, 55, 45

Fig. 1.— The full CCD field, 13.6 x 13.6 arcmin, with North up and East to the left. The more distant RR Lyraes are identified. From a 300s V band exposure with the CTIO 0.9-m telescope.

Fig. 2.— A 100 x 100 arcsec field, with the inner RR Lyraes identified. Otherwise as Figure 1.

Fig. 3.— V magnitude lightcurves as a function of phase for the NGC 1851 RR Lyraes.

Fig. 4.— Log Period vs. log Temperature diagram. Overtone periods have been fundamentalized, and corrections made for luminosity differences, as detailed in the text. The lower four panels show the NGC 1851, IC 4499, NGC 6362 and M68 RR Lyraes, the latter plotted using a reddening of  $E(B-V) = 0.03$ . The top panel superimposes the results for the first three of these clusters. Note that the diagonal reference line is drawn to guide the eye, it is not a fit to the data.

Fig. 5.— Color-magnitude diagram for stars measured within an annulus radii 80 and 260 arcsec.

Fig. 6.— Color-magnitude diagram for stars measured within an annulus radii 30 and 260 arcsec.

Fig. 7.— Color-magnitude diagram for stars in the vicinity of the NGC 1851 Horizontal Branch, measured within an annulus radii 80 and 260 arcsec.

Fig. 8.— Color-magnitude diagram for stars in the vicinity of the NGC 1851 Horizontal Branch, measured within an annulus radii 30 and 260 arcsec.

Table 1. Observing Conditions

Date	Nobs	PM?	Seeing	ColEqn
1993 Aug 23	4	Yes	1''7	A
1993 Nov 29	17	No	1''7	A
30	11	Yes	1''5	A
Dec 1	12	Yes	1''3	A
1994 Mar 7	4	No	1''8	B
8	6	Yes	1''6	B
9	6	Yes	1''5	B
10	3	No	1''7	B
1994 Sep 21	7	Yes	1''6	C
22	7	No	2''5	C
24	8	Yes	1''3	C
25	9	Yes	1''3	C
1994 Nov 23	8	Yes	1''3	D
24	10	Yes	1''5	D
27	14	No	2''0	D

Table 2. Color Equations

Set	$C_V$	$C_{B-V}$	$C_{V-I}$
A	0.027	0.887	1.002
B	0.034	0.899	1.003
C	0.012	0.890	1.000
D	0.012	0.903	1.004

Note. — The color equations are of the form  $V = v + C_V(b - v)$ ,  $B - V = C_{B-V}(b - v)$ ,  $V - I = C_{V-I}(v - i)$ .

Table 3. Constant stars in annulus radii 80, 260 arcsec

Num	X	Y	V	B - V	V - I	$\sigma V$	$\sigma(B - V)$	$\sigma(V - I)$
52	1068.8	1331.1	13.289	0.690	0.727	0.000	0.001	0.001
63	1158.5	704.5	13.399	1.576	1.580	0.001	0.001	0.002
69	1095.6	1141.8	13.473	1.549	1.540	0.001	0.002	0.001
82	434.6	1117.9	13.607	1.482	1.475	0.001	0.001	0.002
90	933.3	1227.7	13.711	1.439	1.439	0.001	0.001	0.001
96	412.1	919.6	13.814	1.482	1.421	0.001	0.001	0.002
97	589.5	841.1	13.807	1.361	1.380	0.001	0.001	0.001
116	1384.7	1239.3	14.029	1.310	1.337	0.001	0.001	0.001
117	1280.1	776.0	14.017	1.333	1.332	0.000	0.001	0.001
126	710.3	822.7	14.135	1.229	1.258	0.001	0.001	0.001
139	856.0	695.2	14.239	1.218	1.261	0.001	0.001	0.001
140	1192.4	331.5	14.272	0.542	0.624	0.001	0.002	0.002
150	753.5	1177.7	14.304	1.287	1.255	0.001	0.001	0.001
159	669.9	1032.9	14.372	1.216	1.254	0.001	0.002	0.001
163	597.2	733.4	14.388	1.184	1.224	0.001	0.002	0.001
169	749.3	1017.7	14.446	1.176	1.221	0.001	0.001	0.001
181	1153.2	830.8	14.531	1.086	1.148	0.001	0.001	0.001
192	1183.5	1043.3	14.573	1.132	1.174	0.001	0.001	0.001
211	1184.7	527.0	14.705	1.098	1.173	0.001	0.001	0.001
212	1169.8	970.4	14.697	0.969	1.064	0.001	0.001	0.001
227	949.8	1155.9	14.771	1.085	1.145	0.001	0.002	0.001
231	867.5	682.8	14.772	0.993	1.037	0.001	0.001	0.001
241	733.0	888.6	14.840	0.968	1.052	0.001	0.001	0.001
243	905.4	604.5	14.836	0.967	1.049	0.001	0.001	0.001
245	775.8	793.3	14.850	0.957	1.011	0.001	0.001	0.001
246	1461.4	1023.0	14.838	1.174	1.136	0.000	0.001	0.001
247	734.5	928.0	14.864	1.056	1.121	0.001	0.001	0.001
249	329.6	864.1	14.850	1.069	1.138	0.001	0.001	0.001
258	1219.8	1320.9	14.914	1.065	1.132	0.000	0.001	0.001
263	1198.6	918.0	14.930	0.917	1.024	0.000	0.001	0.001
264	608.7	1341.7	14.929	1.073	1.142	0.000	0.001	0.001
267	1477.2	1048.5	14.923	0.835	0.889	0.000	0.001	0.001
288	1275.5	1193.2	15.022	1.048	1.119	0.001	0.002	0.001
311	1207.1	798.4	15.104	1.089	1.108	0.000	0.001	0.001
318	1048.0	1134.5	15.125	1.016	1.091	0.001	0.002	0.001
334	1169.1	953.3	15.211	0.991	1.081	0.001	0.002	0.002
339	893.0	729.5	15.190	1.104	1.065	0.001	0.001	0.001
363	1150.7	756.1	15.300	0.604	0.747	0.001	0.001	0.001
367	794.1	797.3	15.303	0.994	1.077	0.001	0.002	0.001
377	1327.0	558.3	15.313	0.997	1.093	0.001	0.001	0.001
395	852.0	1098.6	15.385	0.961	1.049	0.001	0.001	0.001
396	693.7	998.2	15.388	0.779	0.888	0.001	0.001	0.001
400	1079.9	1106.7	15.418	0.940	1.034	0.001	0.002	0.002
407	554.8	472.6	15.416	0.843	0.967	0.001	0.001	0.001
412	1516.7	847.7	15.420	0.991	1.069	0.000	0.001	0.001
427	1346.1	879.3	15.471	0.976	1.048	0.001	0.001	0.001
434	949.1	1174.2	15.489	0.960	1.042	0.001	0.001	0.001

Note. — Table 3 is presented in its entirety in the electronic edition of The Astronomical Journal. A portion is shown here for guidance regarding its form and content.

Table 4. Photometry for NGC 1851-V1

$HJD_V$	phase	$\delta HJD_B$	$\delta HJD_I$	$V$	$B$	$I$	$\sigma_V$	$\sigma_B$	$\sigma_I$
9223.8330	0.434	0.0064	0.0129	16.014	16.044	15.384	0.007	0.016	0.016
9223.8506	0.469	0.0064	0.0128	15.395	15.409	15.194	0.005	0.013	0.016
9223.8691	0.504	0.0066	0.0129	15.310	15.432	15.225	0.005	0.013	0.011
9223.8867	0.537	0.0064	0.0128	15.407	15.566	15.312	0.005	0.006	0.010
9321.7930	0.609	0.0065	0.0130	15.609	15.831	15.415	0.003	0.012	0.007
9321.8105	0.643	0.0096	0.0181	15.700	15.971	15.470	0.004	0.004	0.026
9321.8428	0.705	0.0064	0.0130	15.867	16.160	15.520	0.004	0.007	0.005
9322.5918	0.144	0.0064	0.0130	16.418	16.833	15.872	0.005	0.006	0.006
9322.6113	0.182	0.0067	0.0130	16.449	16.859	15.883	0.006	0.028	0.004
9322.6289	0.217	0.0063	0.0128	16.462	16.877	15.882	0.005	0.038	0.006
9322.6465	0.250	0.0072	0.0137	16.434	16.800	15.892	0.006	0.008	0.017
9322.6660	0.287	0.0063	0.0162	16.448	16.844	15.961	0.006	0.006	0.009
9322.6865	0.326	0.0063	0.0131	16.529	16.952	16.003	0.006	0.005	0.005
9322.7061	0.363	0.0083	0.0147	16.566	16.962	16.001	0.005	0.010	0.009
9322.7314	0.414	0.0082	0.0147	16.407	16.549	15.602	0.005	0.014	0.005
9322.7510	0.449	0.0064	0.0128	15.789	15.762	15.252	0.005	0.007	0.070
9322.7686	0.484	0.0063	0.0127	15.291	15.364	15.183	0.005	0.009	0.032
9322.7861	0.518	0.0063	0.0131	15.303	15.447	15.239	0.005	0.007	0.010
9322.8037	0.553	0.0064	0.0127	15.427	15.595	15.319	0.006	0.007	0.004
9322.8213	0.586	0.0064	0.0127	15.544	15.739	15.380	0.005	0.006	0.004
9323.5791	0.041	0.0063	0.0127	16.413	16.855	15.837	0.005	0.032	0.005
9323.5967	0.074	0.0065	0.0130	16.422	16.830	15.840	0.005	0.004	0.013
9323.6152	0.109	0.0064	0.0134	16.410	16.829	15.846	0.006	0.004	0.005
9323.6338	0.144	0.0063	0.0128	16.412	16.832	15.864	0.007	0.054	0.008
9323.6514	0.180	0.0067	0.0132	16.428	16.851	15.877	0.008	0.015	0.021
9323.6689	0.213	0.0067	0.0133	16.440	16.857	15.875	0.008	0.013	0.004
9323.6885	0.250	0.0064	0.0129	16.406	16.818	15.878	0.007	0.009	0.003
9323.7129	0.297	0.0063	0.0127	16.473	16.913	15.964	0.005	0.005	0.104
9323.7314	0.332	0.0085	0.0155	16.543	16.971	16.004	0.005	0.011	0.043
9323.7510	0.371	0.0071	0.0136	16.565	16.956	15.991	0.007	0.007	0.022
9323.7695	0.406	0.0064	0.0128	16.464	16.723	15.764	0.007	0.006	0.044
9323.7871	0.440	0.0063	0.0127	15.972	15.999	15.362	0.009	0.006	0.009
9323.8037	0.473	0.0065	0.0130	15.395	15.397	15.180	0.006	0.006	0.012
9323.8271	0.518	0.0072	0.0138	15.315	15.465	15.265	0.004	0.022	0.025
9419.5537	0.402	0.0066	0.0134	16.538	16.846	15.836	0.006	0.011	0.004
9419.5723	0.438	0.0066	0.0129	16.130	16.168	15.450	0.005	0.010	0.007
9419.5908	0.473	0.0069	0.0135	15.486	15.454	15.189	0.004	0.013	0.004
9419.6084	0.508	0.0065	0.0126	15.304	15.434	15.227	0.003	0.014	0.005
9419.6270	0.543	0.0064	0.0127	15.404	15.582	15.312	0.003	0.013	0.060
9420.5264	0.270	0.0083	0.0152	16.457	16.887	15.934	0.005	0.011	0.009
9420.5488	0.315	0.0078	0.0144	16.526	17.007	16.018	0.006	0.022	0.011
9420.5869	0.389	0.0063	0.0126	16.578	16.962	15.958	0.013	0.008	0.008
9420.6055	0.422	0.0067	0.0130	16.391	16.549	15.600	0.007	0.008	0.019
9420.6230	0.457	0.0067	0.0130	15.789	15.771	15.256	0.005	0.009	0.013
9420.6406	0.490	0.0123	0.0126	15.334	15.455	15.209	0.005	0.027	0.005
9421.5146	0.168	0.0065	0.0127	16.457	16.903	15.895	0.005	0.013	0.071
9421.5322	0.203	0.0063	0.0127	16.486	16.923	99.999	0.005	0.013	9.999
9421.5674	0.270	0.0065	0.0129	16.462	16.895	15.926	0.005	0.004	0.022
9421.5850	0.305	0.0063	0.0133	16.513	16.960	15.988	0.005	0.014	0.012
9421.6094	0.352	0.0067	0.0131	16.579	17.034	16.029	0.005	0.010	0.111
9421.6270	0.385	0.0064	0.0127	16.576	16.981	15.992	0.005	0.005	0.007
9422.5850	0.225	0.0031	0.0115	16.502	16.936	15.904	0.004	0.005	0.004



Table 4—Continued

$HJD_V$	phase	$\delta HJD_B$	$\delta HJD_I$	$V$	$B$	$I$	$\sigma_V$	$\sigma_B$	$\sigma_I$
9422.6045	0.262	0.0032	0.0115	16.474	16.895	15.907	0.005	0.106	0.005
9422.6221	0.297	0.0032	0.0115	16.473	16.952	15.961	0.007	0.013	0.009
9617.7559	0.137	0.0017	0.0045	16.418	16.844	15.864	0.005	0.017	0.009
9617.7686	0.162	0.0107	0.0136	16.439	16.875	15.874	0.006	0.007	0.006
9617.7910	0.205	0.0073	0.0100	16.473	16.904	15.892	0.005	0.017	0.005
9617.8086	0.238	0.0063	0.0184	16.465	16.875	15.890	0.005	0.006	0.014
9617.8359	0.291	0.0070	0.0133	16.442	16.874	15.913	0.006	0.016	0.054
9619.7461	0.961	0.0064	0.0128	16.334	16.767	15.775	0.005	0.010	0.003
9619.7637	0.994	0.0063	0.0127	16.360	16.815	15.790	0.005	0.018	0.009
9619.8271	0.117	0.0067	0.0129	16.413	16.842	15.838	0.006	0.023	0.007
9619.8516	0.162	0.0063	0.0126	16.442	16.859	15.872	0.005	0.006	0.006
9619.8701	0.197	0.0062	0.0140	16.464	16.897	15.883	0.005	0.005	0.007
9619.8887	0.234	0.0064	0.0126	16.466	16.877	15.879	0.005	0.011	0.026
9620.7568	0.902	0.0062	0.0125	16.245	16.653	15.726	0.005	0.004	0.004
9620.7744	0.935	0.0063	0.0126	16.308	16.729	15.761	0.004	0.043	0.033
9620.7910	0.969	0.0063	0.0127	16.350	16.774	15.785	0.005	0.005	0.060
9620.8125	0.008	0.0063	0.0126	16.383	16.823	15.803	0.005	0.014	0.018
9620.8301	0.041	0.0063	0.0136	16.410	16.841	15.829	0.004	0.005	0.022
9620.8477	0.076	0.0064	0.0129	16.427	16.842	15.836	0.004	0.029	0.015
9620.8652	0.111	0.0063	0.0127	16.423	16.839	15.840	0.005	0.004	0.007
9620.8828	0.143	0.0063	0.0127	16.429	16.845	15.851	0.004	0.005	0.006
9621.7314	0.773	0.0066	0.0129	16.008	16.361	15.598	0.004	0.013	0.040
9621.7490	0.809	0.0107	0.0170	16.080	16.455	15.608	0.005	0.043	0.020
9621.7705	0.850	0.0062	0.0126	16.141	16.523	15.642	0.007	0.007	0.026
9621.7881	0.883	0.0063	0.0127	16.209	16.603	15.688	0.005	0.005	0.009
9621.8057	0.918	0.0064	0.0128	16.269	16.688	15.729	0.004	0.012	0.009
9621.8232	0.951	0.0063	0.0126	16.318	16.751	15.766	0.005	0.007	0.019
9621.8408	0.984	0.0062	0.0123	16.366	16.797	15.793	0.006	0.005	0.017
9621.8574	0.016	0.0062	0.0126	16.399	16.837	15.808	0.006	0.005	0.013
9621.8740	0.049	0.0063	0.0126	16.409	16.846	15.822	0.007	0.022	0.008
9680.6006	0.857	0.0058	0.0116	16.144	16.551	15.668	0.004	0.008	0.029
9680.6162	0.887	0.0058	0.0117	16.194	16.615	15.703	0.003	0.010	0.016
9680.6318	0.918	0.0060	0.0118	16.245	16.680	15.730	0.004	0.011	0.006
9680.6475	0.949	0.0058	0.0116	16.293	16.736	15.752	0.004	0.066	0.055
9680.6641	0.979	0.0058	0.0116	16.328	16.789	15.755	0.005	0.009	0.023
9680.7285	0.103	0.0059	0.0118	16.393	16.838	15.838	0.004	0.004	0.009
9680.7461	0.137	0.0065	0.0123	16.402	16.846	15.850	0.005	0.004	0.012
9680.7617	0.168	0.0060	0.0118	16.412	16.862	15.861	0.005	0.010	0.011
9681.6016	0.781	0.0058	0.0118	16.023	16.376	15.594	0.004	0.005	0.006
9681.6182	0.812	0.0058	0.0118	16.074	16.446	15.627	0.004	0.004	0.023
9681.6338	0.844	0.0058	0.0118	16.131	16.519	15.657	0.004	0.006	0.085
9681.6514	0.877	0.0058	0.0116	16.191	16.601	15.693	0.004	0.006	0.036
9681.6670	0.906	0.0058	0.0117	16.239	16.665	15.721	0.004	0.010	0.011
9681.6826	0.938	0.0058	0.0117	16.295	16.730	15.764	0.004	0.037	0.009
9681.6992	0.967	0.0058	0.0117	16.344	16.784	15.777	0.005	0.016	0.006
9681.7148	0.998	0.0059	0.0119	16.376	16.826	15.810	0.005	0.022	0.018
9681.7402	0.047	0.0058	0.0119	16.404	16.852	15.832	0.004	0.004	0.007
9681.7559	0.078	0.0058	0.0119	16.421	16.866	15.844	0.004	0.028	0.007
9684.5537	0.451	0.0066	0.0128	16.022	16.088	15.400	0.003	0.016	0.049
9684.5703	0.484	0.0061	0.0122	15.449	15.477	15.190	0.002	0.006	0.015
9684.5869	0.516	0.0058	0.0116	15.289	15.440	15.215	0.002	0.037	0.020
9684.6025	0.545	0.0058	0.0116	15.368	15.552	15.279	0.002	0.020	0.028

Table 4—Continued

$HJD_V$	phase	$\delta HJD_B$	$\delta HJD_I$	$V$	$B$	$I$	$\sigma_V$	$\sigma_B$	$\sigma_I$
9684.6270	0.592	0.0062	0.0143	15.526	15.745	15.373	0.002	0.004	0.015
9684.6484	0.635	0.0062	0.0125	15.658	15.915	15.432	0.003	0.003	0.012
9684.6660	0.666	0.0060	0.0119	15.750	16.029	15.467	0.003	0.002	0.009
9684.6816	0.697	0.0059	0.0131	15.832	16.137	15.512	0.003	0.010	0.046
9684.7021	0.736	0.0058	0.0119	15.925	16.261	15.556	0.003	0.004	0.005
9684.7188	0.768	0.0061	0.0123	15.987	16.348	15.589	0.003	0.004	0.010
9684.7354	0.801	0.0058	0.0119	16.047	16.423	15.613	0.003	0.023	0.038
9684.7510	0.830	0.0061	0.0122	16.103	16.497	15.647	0.003	0.005	0.017
9684.7686	0.865	0.0058	0.0120	16.166	16.583	15.687	0.003	0.006	0.015

Note. — Table 4 is presented in its entirety in the electronic edition of The Astronomical Journal. A portion is shown here for guidance regarding its form and content.

Table 5. Periods and mean magnitudes for the RR Lyrae variables

Var	Num	Period(d)	$\langle V \rangle$	$\langle B \rangle$	$\langle I \rangle$	$(B - V)_m$	$(V - I)_m$	$A_V$	$A_B$	$A_I$
1	628	0.520578	16.050	16.340	15.646	0.339	0.451	1.37	1.70	0.87
3	586	0.322152	16.054	16.307	15.712	0.261	0.352	0.48	0.64	0.28
4	703	0.585110	16.127	16.489	15.641	0.393	0.571	0.98	1.28	0.59
5	702	0.587860	16.039	16.404	15.554	0.386	0.499	0.67	0.88	0.45
6	661	0.606623	16.092	16.473	15.589	0.404	0.521	0.88	1.13	0.55
7	701	0.585185	16.044	16.380	15.582	0.376	0.492	1.11	1.45	0.71
8	603	0.511000	16.072	16.334	15.696	0.320	0.429	1.26	1.60	0.73
10	684	0.499750	16.119	16.454	15.719	0.360	0.419	0.62	0.82	0.34
11	486	0.667930	15.937	16.321	15.430	0.405	0.523	0.82	1.06	0.51
12	673	0.575960	16.122	16.488	15.632	0.392	0.511	0.96	1.24	0.61
13	626	0.282540	16.118	16.343	15.845	0.233	0.283	0.59	0.68	0.36
14	418	0.594010	15.429	15.919	14.762	0.484	0.672	0.80	0.91	0.40
15	749	0.541320	16.016	16.311	15.612	0.338	0.446	1.30	1.63	0.89
16	575	0.488690	16.107	16.394	15.712	0.333	0.438	1.19	1.49	0.75
17	612	0.700307	16.101	16.419	15.454	0.427	0.554	0.53	0.68	0.35
18	544	0.272091	16.067	16.295	15.784	0.237	0.293	0.51	0.65	0.31
19	505	0.405161	15.851	16.148	15.488	0.302	0.364	0.47	0.56	0.40
20	517	0.559470	15.935	16.288	15.457	0.376	0.493	0.74	1.06	0.49
21	647	0.268521	16.111	16.328	15.851	0.226	0.269	0.50	0.63	0.30
22	753	0.559390	16.084	16.391	15.562	0.343	0.539	0.98	1.20	0.64
23	688	0.265830	16.112	16.324	15.853	0.214	0.262	0.26	0.32	0.17
26	710	0.328683	16.111	16.399	15.746	0.296	0.374	0.46	0.59	0.28
27	919	0.523230	16.084	16.412	15.720	0.375	0.412	1.02	1.27	0.70
28	654	0.646670	16.082	16.480	15.540	0.415	0.556	0.68	0.92	0.42
29	646	0.603530	15.991	16.379	15.518	0.402	0.488	0.82	0.90	0.55
30	448	0.539400	15.868	16.084	15.306	0.350	0.450	0.90	1.30	0.50
31	572	0.426653	15.964	16.378	15.457	0.426	0.522	0.61	0.71	0.40
32	764	0.659708	16.119	16.515	15.605	0.405	0.519	0.53	0.67	0.34
33	648	0.341231	16.121	16.383	15.843	0.273	0.300	0.53	0.67	0.26

Table 6. RR Lyrae Fourier parameters

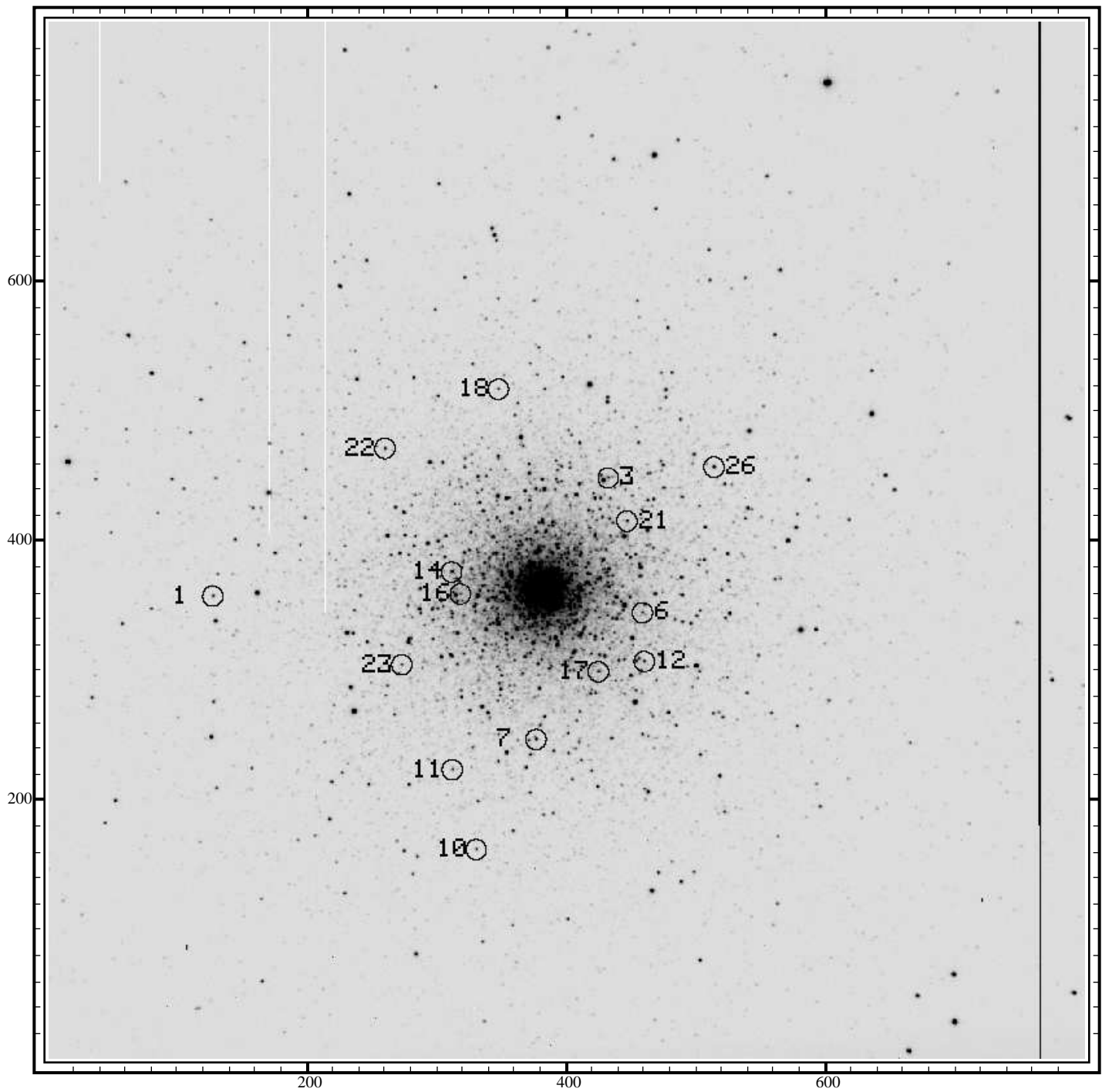
Var	Num	Filt	$A_0$	$\sigma A_0$	$A_1$	$\sigma A_1$	$R_{21}$	$\sigma R_{21}$	$R_{31}$	$\sigma R_{31}$	$R_{41}$	$\sigma R_{41}$	$\phi_1$	$\sigma(\phi_1)$	$\phi_{21}$	$\sigma(\phi_{21})$
3	586	V	16.069	0.002	0.252	0.003	0.108	0.012	0.074	0.012	0.053	0.012	3.43	0.01	4.50	0.12
3	586	B	16.330	0.002	0.318	0.003	0.095	0.009	0.079	0.008	0.046	0.008	3.56	0.01	4.48	0.10
3	586	I	15.717	0.002	0.146	0.004	0.126	0.027	0.061	0.025	0.062	0.025	3.60	0.02	4.83	0.23
13	626	V	16.139	0.007	0.281	0.009	0.180	0.039	0.033	0.034	0.048	0.034	0.25	0.03	4.81	0.25
13	626	B	16.372	0.006	0.344	0.008	0.159	0.026	0.056	0.024	0.080	0.024	0.37	0.02	5.03	0.19
13	626	I	15.856	0.010	0.183	0.014	0.135	0.087	0.140	0.090	0.033	0.078	0.55	0.08	5.67	0.71
18	544	V	16.083	0.001	0.256	0.002	0.197	0.009	0.055	0.008	0.059	0.008	5.16	0.01	4.74	0.05
18	544	B	16.320	0.002	0.322	0.003	0.189	0.010	0.049	0.009	0.053	0.009	5.29	0.01	4.68	0.06
18	544	I	15.790	0.002	0.150	0.002	0.226	0.020	0.052	0.017	0.044	0.017	5.37	0.02	4.88	0.11
19	505	V	15.865	0.008	0.225	0.012	0.114	0.058	0.078	0.056	0.003	0.052	6.01	0.05	4.68	0.56
19	505	B	16.167	0.006	0.274	0.008	0.037	0.030	0.076	0.031	0.057	0.031	6.09	0.03	4.06	0.84
19	505	I	15.501	0.012	0.170	0.017	0.145	0.111	0.162	0.113	0.105	0.106	6.23	0.09	4.38	0.86
21	647	V	16.126	0.002	0.250	0.003	0.207	0.013	0.053	0.011	0.052	0.011	3.42	0.01	4.64	0.07
21	647	B	16.352	0.002	0.315	0.002	0.187	0.009	0.041	0.008	0.056	0.007	3.55	0.01	4.71	0.05
21	647	I	15.857	0.002	0.150	0.003	0.205	0.023	0.062	0.020	0.068	0.020	3.64	0.02	4.65	0.13
23	688	V	16.117	0.005	0.124	0.006	0.081	0.057	0.018	0.054	0.029	0.054	5.67	0.05	4.98	0.75
23	688	B	16.331	0.006	0.154	0.008	0.085	0.059	0.013	0.055	0.029	0.056	5.78	0.05	4.67	0.74
23	688	I	15.855	0.003	0.077	0.004	0.113	0.063	0.005	0.058	0.062	0.059	5.96	0.06	4.38	0.61
26	710	V	16.124	0.002	0.237	0.003	0.063	0.012	0.082	0.013	0.031	0.011	2.10	0.01	4.96	0.22
26	710	B	16.420	0.002	0.301	0.003	0.082	0.012	0.082	0.012	0.043	0.011	2.25	0.01	4.72	0.16
26	710	I	15.750	0.002	0.142	0.003	0.061	0.019	0.076	0.020	0.046	0.019	2.22	0.02	5.22	0.35
31	572	V	15.990	0.012	0.279	0.017	0.233	0.072	0.056	0.062	9.999	9.999	3.23	0.06	4.90	0.38
31	572	B	16.415	0.014	0.339	0.020	0.188	0.068	0.099	0.063	9.999	9.999	3.32	0.06	4.74	0.43
31	572	I	15.469	0.009	0.173	0.013	0.292	0.097	0.098	0.081	9.999	9.999	3.17	0.07	5.14	0.41
33	648	V	16.223	0.011	0.238	0.014	0.195	0.077	0.132	0.070	9.999	9.999	0.28	0.07	0.45	0.45
33	648	B	16.477	0.010	0.336	0.014	0.122	0.044	0.159	0.046	9.999	9.999	0.49	0.04	5.54	0.46
33	648	I	15.919	0.019	0.086	0.026	0.554	0.447	0.541	0.465	9.999	9.999	0.58	0.32	5.12	1.28
1	628	V	16.124	0.004	0.452	0.006	0.478	0.019	0.341	0.017	0.215	0.015	5.48	0.01	3.91	0.05
1	628	B	16.463	0.005	0.579	0.007	0.474	0.018	0.332	0.016	0.204	0.015	5.60	0.01	3.82	0.05
1	628	I	15.673	0.002	0.269	0.003	0.504	0.018	0.382	0.016	0.251	0.015	5.45	0.01	4.26	0.05
4	703	V	16.164	0.005	0.315	0.007	0.566	0.035	0.334	0.030	0.215	0.027	1.40	0.02	3.99	0.08
4	703	B	16.557	0.007	0.433	0.010	0.523	0.035	0.344	0.031	0.204	0.027	1.56	0.02	3.76	0.09
4	703	I	15.653	0.005	0.180	0.008	0.652	0.070	0.330	0.057	0.219	0.051	1.24	0.04	4.49	0.15
5	702	V	16.063	0.010	0.259	0.015	0.440	0.082	0.267	0.070	0.142	0.064	0.56	0.05	4.22	0.23
5	702	B	16.449	0.013	0.364	0.019	0.348	0.070	0.250	0.063	0.120	0.055	0.68	0.05	4.12	0.25
5	702	I	15.564	0.007	0.147	0.011	0.679	0.122	0.221	0.085	0.142	0.073	0.55	0.07	4.42	0.24
6	661	V	16.123	0.002	0.297	0.004	0.524	0.018	0.326	0.016	0.177	0.014	5.08	0.01	4.10	0.04
6	661	B	16.528	0.003	0.396	0.005	0.504	0.017	0.303	0.015	0.168	0.014	5.21	0.01	3.96	0.04
6	661	I	15.602	0.003	0.188	0.004	0.525	0.030	0.294	0.025	0.153	0.022	4.96	0.02	4.57	0.07
7	701	V	16.095	0.001	0.363	0.002	0.520	0.009	0.333	0.007	0.233	0.007	3.43	0.01	3.99	0.02
7	701	B	16.471	0.003	0.485	0.004	0.498	0.012	0.333	0.010	0.215	0.009	3.54	0.01	3.91	0.03
7	701	I	15.601	0.001	0.220	0.002	0.527	0.015	0.356	0.012	0.251	0.012	3.34	0.01	4.35	0.04
8	603	V	16.151	0.008	0.463	0.011	0.456	0.033	0.321	0.030	0.180	0.027	0.60	0.02	3.63	0.10
8	603	B	16.471	0.010	0.609	0.015	0.452	0.034	0.294	0.031	0.164	0.028	0.67	0.02	3.72	0.10
8	603	I	15.722	0.008	0.270	0.011	0.425	0.056	0.267	0.050	0.226	0.048	0.64	0.04	3.93	0.18
11	486	V	15.964	0.003	0.287	0.004	0.515	0.021	0.326	0.019	0.109	0.016	3.17	0.02	4.17	0.07
11	486	B	16.369	0.003	0.382	0.003	0.504	0.015	0.307	0.013	0.106	0.011	3.30	0.01	4.05	0.05
11	486	I	15.441	0.003	0.182	0.004	0.480	0.034	0.317	0.032	0.102	0.027	3.10	0.03	4.46	0.12
12	673	V	16.157	0.002	0.319	0.003	0.508	0.014	0.332	0.012	0.215	0.011	3.15	0.01	4.04	0.04
12	673	B	16.549	0.003	0.417	0.003	0.512	0.012	0.331	0.011	0.208	0.010	3.29	0.01	3.86	0.03
12	673	I	15.646	0.002	0.199	0.002	0.532	0.019	0.320	0.017	0.219	0.016	3.06	0.01	4.40	0.05
14	418	V	15.431	0.032	0.262	0.044	0.347	0.222	0.148	0.142	0.302	0.131	1.00	0.16	5.25	0.65

Table 6—Continued

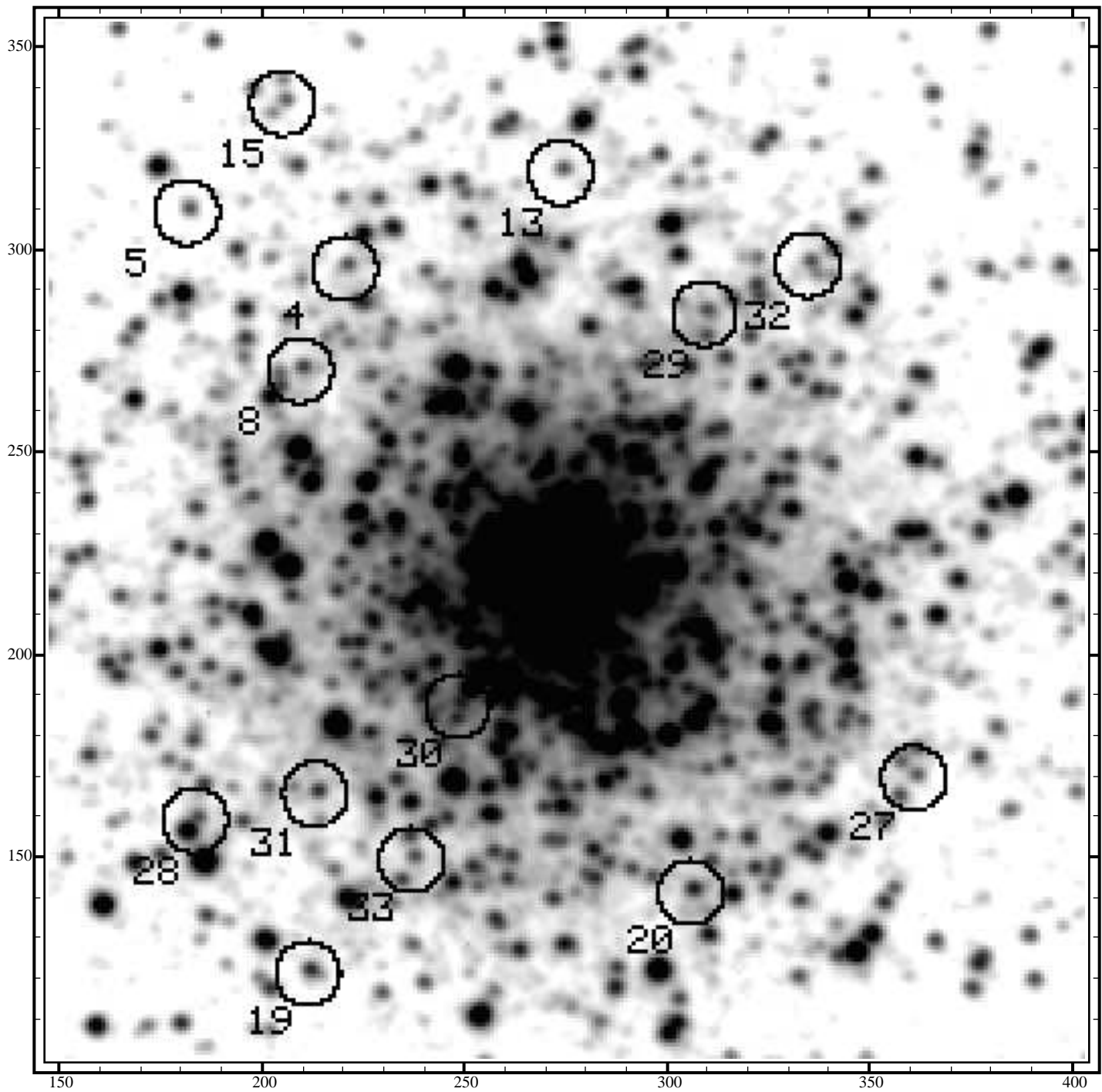
Var	Num	Filt	$A_0$	$\sigma A_0$	$A_1$	$\sigma A_1$	$R_{21}$	$\sigma R_{21}$	$R_{31}$	$\sigma R_{31}$	$R_{41}$	$\sigma R_{41}$	$\phi_1$	$\sigma(\phi_1)$	$\phi_{21}$	$\sigma(\phi_{21})$
14	418	B	15.915	0.038	0.316	0.052	0.332	0.152	0.137	0.116	0.263	0.110	1.12	0.15	4.53	0.82
14	418	I	14.759	0.029	0.115	0.040	0.512	0.538	0.102	0.254	0.291	0.250	1.00	0.33	5.41	1.03
15	749	V	16.086	0.007	0.434	0.011	0.519	0.036	0.355	0.032	0.184	0.028	3.29	0.02	3.82	0.09
15	749	B	16.424	0.008	0.545	0.011	0.519	0.031	0.348	0.027	0.200	0.024	3.40	0.02	3.72	0.08
15	749	I	15.640	0.005	0.269	0.007	0.554	0.040	0.370	0.035	0.264	0.032	3.28	0.02	4.16	0.09
16	575	V	16.175	0.005	0.451	0.007	0.461	0.021	0.283	0.019	0.138	0.017	2.75	0.01	3.92	0.06
16	575	B	16.508	0.005	0.587	0.008	0.446	0.019	0.253	0.016	0.131	0.015	2.84	0.01	3.85	0.06
16	575	I	15.737	0.003	0.271	0.005	0.473	0.025	0.297	0.022	0.149	0.020	2.76	0.02	4.20	0.07
17	612	V	16.014	0.002	0.210	0.003	0.440	0.021	0.215	0.019	0.092	0.016	2.54	0.02	4.33	0.07
17	612	B	16.441	0.002	0.274	0.003	0.436	0.016	0.220	0.014	0.067	0.012	2.68	0.01	4.07	0.05
17	612	I	15.460	0.002	0.137	0.003	0.435	0.032	0.212	0.028	0.102	0.025	2.37	0.02	4.71	0.10
20	517	V	15.962	0.008	0.281	0.011	0.431	0.055	0.273	0.048	0.156	0.046	4.99	0.04	3.89	0.19
20	517	B	16.338	0.008	0.375	0.011	0.480	0.043	0.294	0.037	0.186	0.036	5.09	0.03	3.99	0.13
20	517	I	15.469	0.009	0.166	0.011	0.547	0.104	0.294	0.087	0.212	0.086	4.84	0.08	4.60	0.29
22	753	V	16.125	0.009	0.365	0.013	0.483	0.049	0.275	0.046	0.137	0.036	2.49	0.04	3.92	0.15
22	753	B	16.468	0.012	0.497	0.016	0.440	0.042	0.200	0.039	0.082	0.032	2.63	0.03	3.82	0.15
22	753	I	15.586	0.020	0.266	0.023	0.287	0.133	0.178	0.090	0.139	0.082	2.62	0.13	4.15	0.55
27	919	V	16.157	0.014	0.406	0.019	0.438	0.046	0.233	0.050	0.139	0.030	6.00	0.05	3.90	0.23
27	919	B	16.532	0.017	0.512	0.024	0.422	0.043	0.249	0.050	0.116	0.031	5.98	0.05	3.83	0.23
27	919	I	15.745	0.016	0.232	0.022	0.480	0.090	0.365	0.112	0.238	0.075	5.80	0.09	4.08	0.43
28	654	V	16.104	0.006	0.257	0.009	0.475	0.051	0.264	0.043	0.092	0.038	3.09	0.04	4.13	0.14
28	654	B	16.519	0.009	0.337	0.012	0.539	0.056	0.245	0.045	0.093	0.039	3.19	0.04	4.03	0.14
28	654	I	15.548	0.006	0.146	0.008	0.568	0.092	0.218	0.072	0.149	0.064	2.94	0.06	4.63	0.23
29	646	V	16.011	0.010	0.288	0.015	0.534	0.079	0.234	0.062	9.999	9.999	1.36	0.04	4.06	0.18
29	646	B	16.409	0.011	0.367	0.016	0.427	0.062	0.242	0.052	9.999	9.999	1.53	0.04	3.72	0.17
29	646	I	15.511	0.013	0.154	0.019	0.369	0.154	0.554	0.181	9.999	9.999	1.08	0.11	5.22	0.55
30	448	V	15.964	0.053	0.390	0.076	0.426	0.273	0.190	0.205	9.999	9.999	3.35	0.17	3.41	0.79
30	448	B	16.203	0.063	0.396	0.091	0.520	0.334	0.511	0.317	9.999	9.999	3.29	0.21	3.89	0.86
30	448	I	15.355	0.054	0.179	0.083	0.486	0.656	0.313	0.541	9.999	9.999	3.15	0.38	5.01	1.66

Table 7. Instability Strip Boundaries

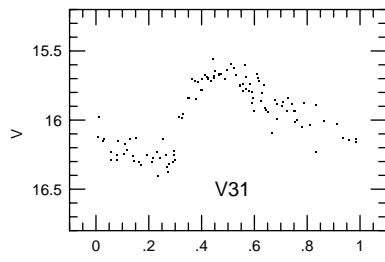
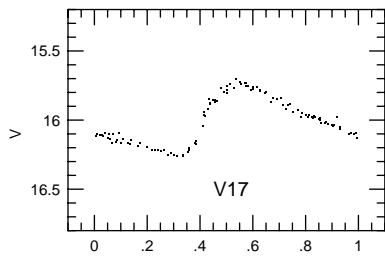
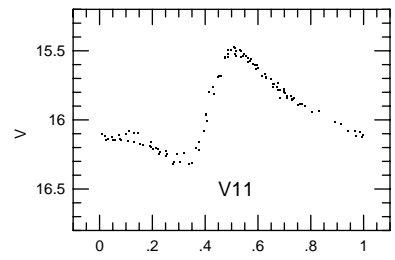
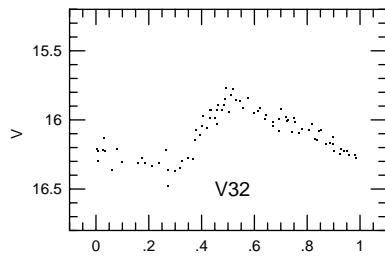
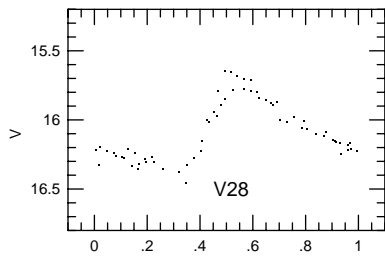
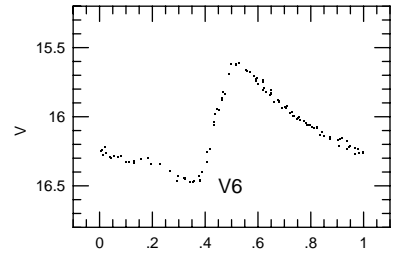
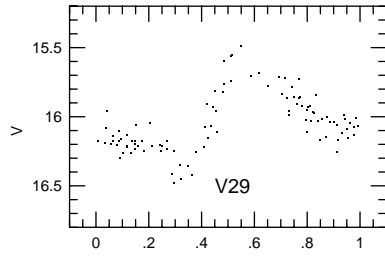
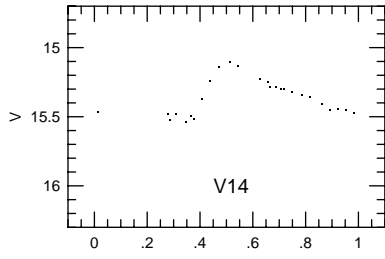
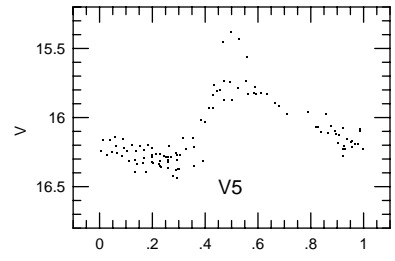
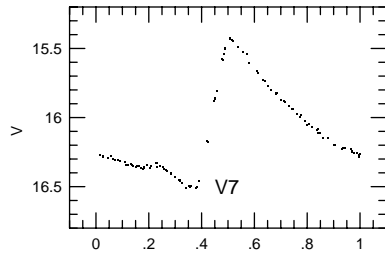
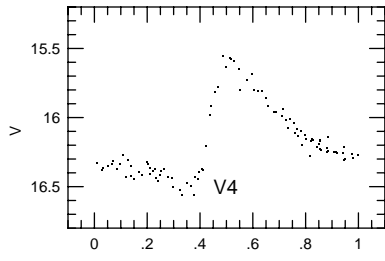
Cluster	[Fe/H]	E(B-V)	$B - V_{HBE}$	$B - V_{FRE}$	$B - V_T$
6362	-1.1	0.04	0.18	0.44	0.28
1851	-1.3	0.02	0.19	0.41	0.29
4499	-1.6	0.22	0.17	0.39	0.29
M72	-1.6	0.05	0.18	0.39	0.28
Ret.	-1.7	0.03	0.17	0.40	0.28
2257	-1.8	0.04	0.18	0.37	0.28
1466	-1.8	0.09	0.16	0.42	0.27
1841	-2.2	0.18	0.18	0.37	..
M68	-2.2	0.07	0.17	0.39	0.28











PHASE

PHASE

PHASE

